Structural characterization of nano-scale precipitates in Cu bearing extra-low-carbon steels

Taeg-Woo Lee [a], Sung-Il Kim [b], Moon-Hi Hong [c], Won-Yong Kim [d], Sung-Hwan Lim [a],*

[a] Department of Advanced Materials Science and Engineering, Kangwon National University, Chuncheon 200-701, South Korea
[b] POSCO Technical Research Laboratories, Gwangyang, Jeonnam 545-090, South Korea
[c] POSCO Gwangyang Steelworks, Jeonnam 545-700, South Korea
[d] Advanced Material Processing Team, Korea Institute of Industrial Technology, Incheon 406-800, South Korea

ARTICLE INFO

ABSTRACT

The morphologies, size distributions, and crystal structures of sulfide and nitride precipitates in the copper (Cu) bearing extra-low-carbon steel matrix were investigated by transmission electron microscopy (TEM) coupled with energy-dispersive X-ray spectrometry (EDS). An atomic-scale structural analysis by high-resolution electron microscopy (HREM) also was carried out. The (Cu, Mn)S precipitates manifested a core–shell structure, the shell part containing Cu and S elements, and the core part Mn and S elements. Most of the nano-scale nitrides of wurtzite structure were less than 30 nm in diameter; indeed, the average diameter as estimated was about 20 nm. The TEM analysis also revealed two nitride precipitation modes: hexagonal AlN precipitates of relatively large size (several tens of nm) and elongated/cuboidal morphology, and cubic TiN precipitates of square and rectangular shape.

1. Introduction

Further to reports of the existence of copper sulfide and nitride in strip-cast steel, these small-diameter precipitates have been found to increase overall steel strength. Extensive experimental investigations into copper sulfide and nitride precipitation resulting from thermal aging in low-carbon steels containing copper (Cu) and nitrogen (N) have been conducted [1,2].

Cu, one of the major residual elements in steel, is not easily removed during the steelmaking process. Although Cu causes rephrasing/segmentation under high-temperature conditions owing to the typical oxidation of the iron (Fe) matrix and its own densification on steel surfaces, it is not taken into the oxide phase but remains in the Fe matrix, due to the fact that its oxidation tendency is weaker than that of Fe. Therefore, Cu can be used as an alloying element in steels to improve their corrosion resistance and enhance their mechanical properties [3]. Cu in steel causes hot shortness, but fine Cu precipitates improve steel performance [4,5]. Solving the problem of hot shortness while retaining the advantages of Cu precipitation requires that the behavior of Cu precipitation in Fe–Cu alloys be properly understood.

Some investigations [6], by contrast, have reported that AlN has no influence on the hot ductility of steel. The most significant effect of AlN in steel is grain-size control [7,8], which directly influences mechanical properties. The size of Al or Ti nitrides fluctuates over a large range, from several nanometers to several tens of nanometers, according to chemical composition, heat treatment, and steel processing conditions [9]. Moreover, AlN and TiN nitrides appear in more than one crystallographic form in steel.

In the present study, the alloying elements Cu and N were added to Cu bearing extra-low-carbon steels in minimal quantities, and resultant improvements in the steels' mechanical properties were confirmed. The morphologies, size distributions, and crystal structures of the precipitates in the steel matrix were investigated by transmission electron microscopy (TEM). It was determined that the precipitates' microstructures include a mechanism that under certain processing conditions can significantly improve the mechanical properties of Cu bearing extra-low-carbon steels.

2. Experimental procedure

Table 1 lists the chemical compositions of the steels as prepared by laboratory vacuum-induction melting. The specimens were square as-cast slabs of 60 mm thickness, 170 mm width, and 200 mm length. After 1200 °C furnace homogenization, the specimens were subjected to a hot-rolling. Specially, the slabs were fed into a rolling mill and passed through seven times, producing 3.2 mm-thick hot sheets. The rolling temperature at finishing was about 900 °C. The surface temperature of the slabs during the rolling test was measured by pyrometer. After rolling, the hot

* Corresponding author. Tel.: +82 33 250 6267; fax: +82 33 250 6260.
  E-mail address: shlim@kangwon.ac.kr (S.-H. Lim).

Table 1
Chemical compositions of steels.

Element (wt.%)	C	Mn	P	S	B	Cu	N	Nb	Al	Ti	Si
Steel A	0.0018	0.136	0.0543	0.0091	0.005	0.079	0.0014	0.002	0.0638	0.0015	0.0454
Steel B	0.0019	0.141	0.0532	0.009	0.005	0.078	0.0014	0.0019	0.0638	0.0015	0.04
Steel C	0.0016	0.144	0.055	0.0085	–	0.06	0.002	0.001	0.046	0.004	0.055

Table 2
Measured mechanical properties of steels.

Type	Yield strength (MPa)	Tensile strength (MPa)	Elongation (%)	Aging index	Bake hardening (MPa)
Steel A	236	356	39	1	75
Steel B	221	342	40	2	69
Steel C	240	347	42	0	62

Table 3
Nucleation rates of MnS and Cu_2S for the various temperatures [3].

	Heterogeneous				Homogeneous			
	MnS in α-Fe	MnS in γ-Fe	Cu_2S in α-Fe	Cu_2S in γ-Fe	MnS in α-Fe	MnS in γ-Fe	Cu_2S in α-Fe	Cu_2S in γ-Fe
900 K	10^{-20}	–	10^{25}	–	10^{-105}	–	10^{25}	–
1000 K	10^{-30}	10	10^{25}	10^{15}	–	10^{-45}	10^{25}	10^{-30}
1100 K	10^{-40}	10^{-5}	10^{25}	10^{10}	–	10^{-60}	10^{25}	10^{-40}
1200 K	10^{-65}	10^{-15}	–	10	–	10^{-85}	10^{25}	10^{-70}
1300 K	–	10^{-30}	–	10^{-30}	–	–	–	–
1400 K	–	10^{-60}	–	–	–	–	–	–

bands were cooled by a water cooling system. In an investigation of the coiling temperature effect, the coiling temperature of steels A and B was increased from 500 to 600 °C. The hot-rolled sheets were then cold-rolled into 0.7 mm thicknesses, after which they were annealed at 800 °C in an infrared furnace.

Preparatory to a conventional high-resolution TEM analysis of the chemical compositions, distributions and atomic structures of the various precipitates, thin-sliced specimens were cut from the bulk to a thickness of 1 mm and mechanically ground to approximately 50 μm, and then electro-polished in an electrochemical solution containing 7 ml perchloric acid and 1000 ml acetic acid, and held at 17 °C under 21 V, yielding foil samples of 3 mm diameter. TEM carbon extraction replica specimens were prepared according to the conventional procedure for measuring the average size and surface density of precipitates. Due to the irregular thickness of the thin foil specimens, the bulk density calculations incurred errors. On the other hand, the precipitates' surface density calculations from the carbon extraction replica specimens were error-free, owing to the same surface conditions of specimens. The measured surface density was the average value derived from 20 randomly selected areas of the carbon extraction replica specimens. A JEOL-2100F TEM equipped with an energy-dispersive X-ray spectroscopy (EDS) detector and operating at 200 kV was employed in the analysis.

3. Results and discussion

Fig. 1 shows the average diameters and surface densities of the precipitates in steels A, B, and C. The precipitates in each sample were less than 20 nm in diameter; the average diameters were 6.00 nm, 14.60 nm, and 6.55 nm, respectively. Steel C had the highest surface density, and its precipitates were distributed more
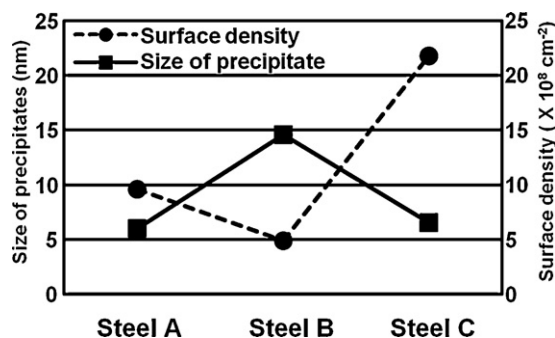

Fig. 1. Average sizes and surface densities of precipitates.

uniformly and densely than those of steels A or B. Table 2 shows also that steel C had the highest yield strength and the greatest elongation. Steel C contained a lower amount of Al than the other steels, and accordingly, the N was lower precipitated as AlN. Additionally, the diffusion coefficient of solute N in the ferrite matrix did not differ much from that of solute C, and the solubility limit of N is higher than that of C. Thus, it would be expected that solute N is another major factor affecting yield strength and elongation, if N is not completely precipitated as nitrides by the addition of Ti and Al [10]. In each sample, Mn-containing precipitates were randomly distributed in the matrix. The largest precipitates in steels A, B and C were the coarse spherical (Cu, Mn)S, characterized as Mn-containing face-centered cubic Cu_2S precipitates, and understood in terms of their calculated activation energy and critical nucleation radius. Liu et al. [3] reported that the activation energy and the critical nucleation radius of Cu_2S were only slightly lower and smaller than those of MnS. As such, Cu_2S precipitates were the largest sulfides. Takahashi [5] reported that yield strength and tensile strength increase in direct proportion to increasing Cu content. This can be explained by the fact that Cu addition under high-temperature conditions suppresses austenite–ferrite transformation by way of the solute Cu in austenite, which suppression prevents ferrite grain growth and retards recrystallization of hot-deformed austenite by the solute Cu, which retardation, in turn, enhances ferrite nucleation. Contributory to the improved yield and tensile strengths as well is the grain-refinement resulting from Cu addition.

Fig. 2 shows bright-field TEM micrographs of the various precipitates in steels A, B and C. The micrographs, obtained from the extraction replica specimens, show the two sulfide precipitation modes: fine (Cu_xS) and coarse ((Cu, Mn)S) spherical precipitates. These precipitates have arbitrary spherical shapes and range between 10 and 200 nm in size. The micrographs also revealed two additional nitride precipitation modes: AlN precipitates of relatively large size (several tens of nm) and elongated/cuboidal morphology (Fig. 3a), and TiN (a different nitride family) precipitates of square and rectangular shapes (Fig. 3b). Fig. 3a and b show typical HREM images of AlN and TiN precipitates. The incident electron beams were parallel to the [2 −1 −1 0], and [0 0 1] direc-
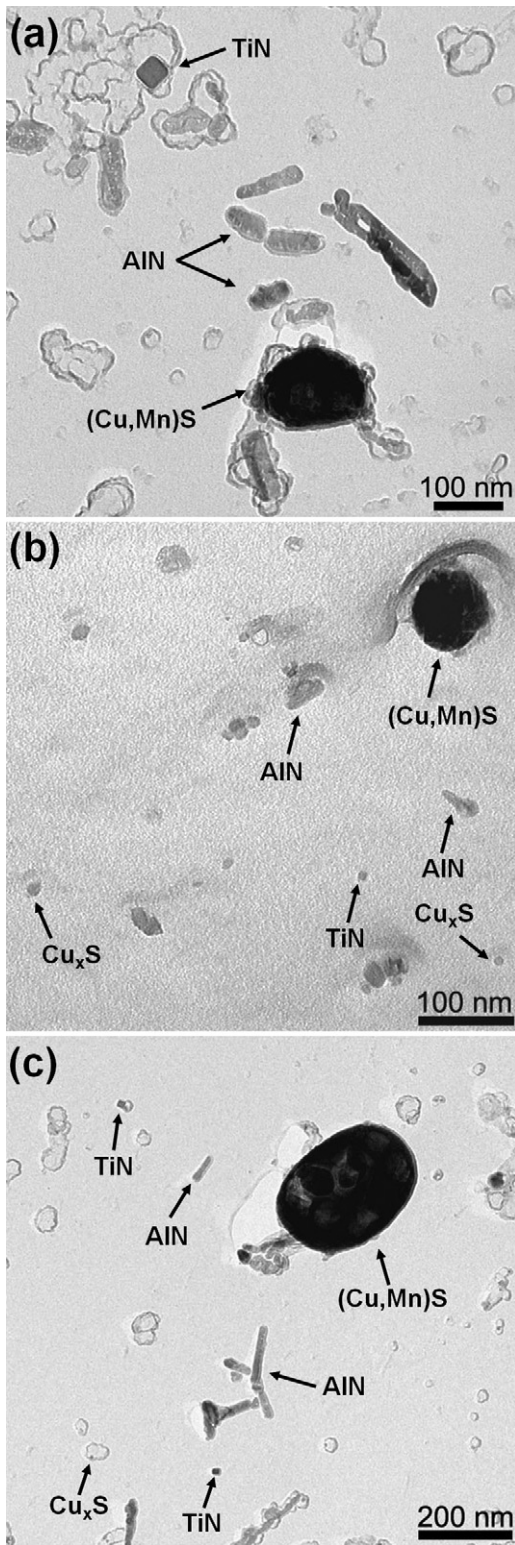
Fig. 2. Morphologies of various sulfides and nitrides in (a) steel A, (b) steel B and (c) steel C.

Fig. 3. High-resolution lattice images of (a) AlN and (b) TiN precipitates in steel B.

tions, respectively. The corresponding Fourier Transforms (insets of Fig. 3a and b) are indexed to the hexagonal (wurtzite) and cubic structures, respectively. Both precipitates, AlN and TiN, were clearly visible when their large faces were perpendicular to the electron beam.

In steel B, precipitates of core–shell structure also were found. Fig. 4 illustrates the results of an EDS elemental mapping and line
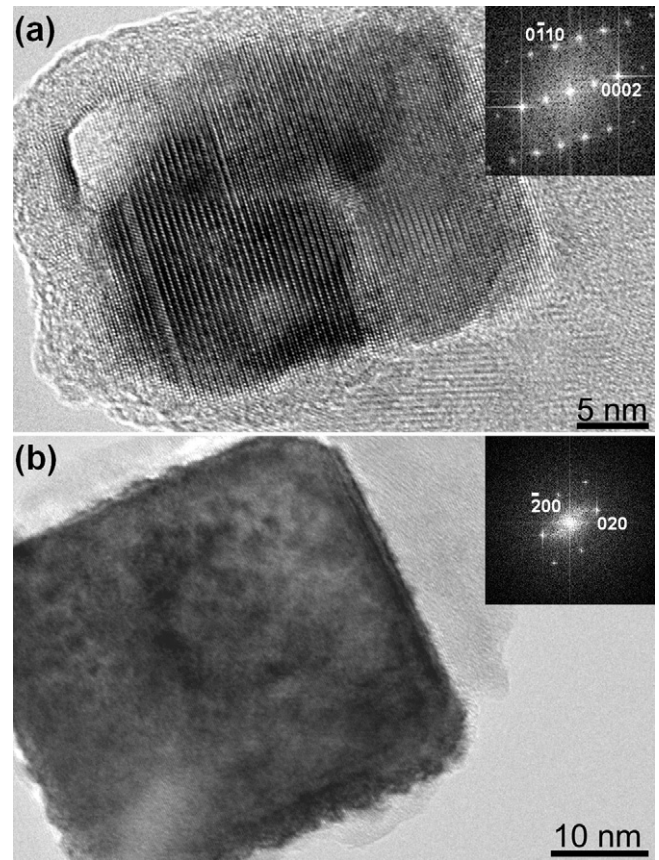
scanning analysis of the core–shell (Cu, Mn)S. The Cu elements were observed to have a higher intensity than the Mn elements in the shell-part (the area between the solid line and the dotted line in Fig. 4e), but the Mn elements were found only in the core-part (the area inside the solid line in Fig. 4c and e), and the S elements were observed in both the core- and shell-parts. That is, the Cu and S elements were distributed in the shell, and the Mn and S elements in the core. At high temperatures, MnS has a larger nucleation driving force than Cu_2S, but at low temperatures (below 1373 K), the opposite is true in both γ-Fe and α-Fe [11]. It was determined that there is homogeneous nucleation in the steel matrix and heterogeneous nucleation on the grain boundary. As shown in Tables 3 and 4 [3], the heterogeneous nucleation rate of MnS is very low due to the high interfacial energy in α-Fe, whereas that of Cu_2S is much higher due to the low interfacial energy. With regard to homogeneous nucleation in the steel matrix, only that of Cu_2S in α-Fe is likely, since the rate was found to be almost in the same range as that of Cu_2S on the grain boundary. This calculation implies that

Table 4
Interfacial energies between steel matrix and some sulfides [3].

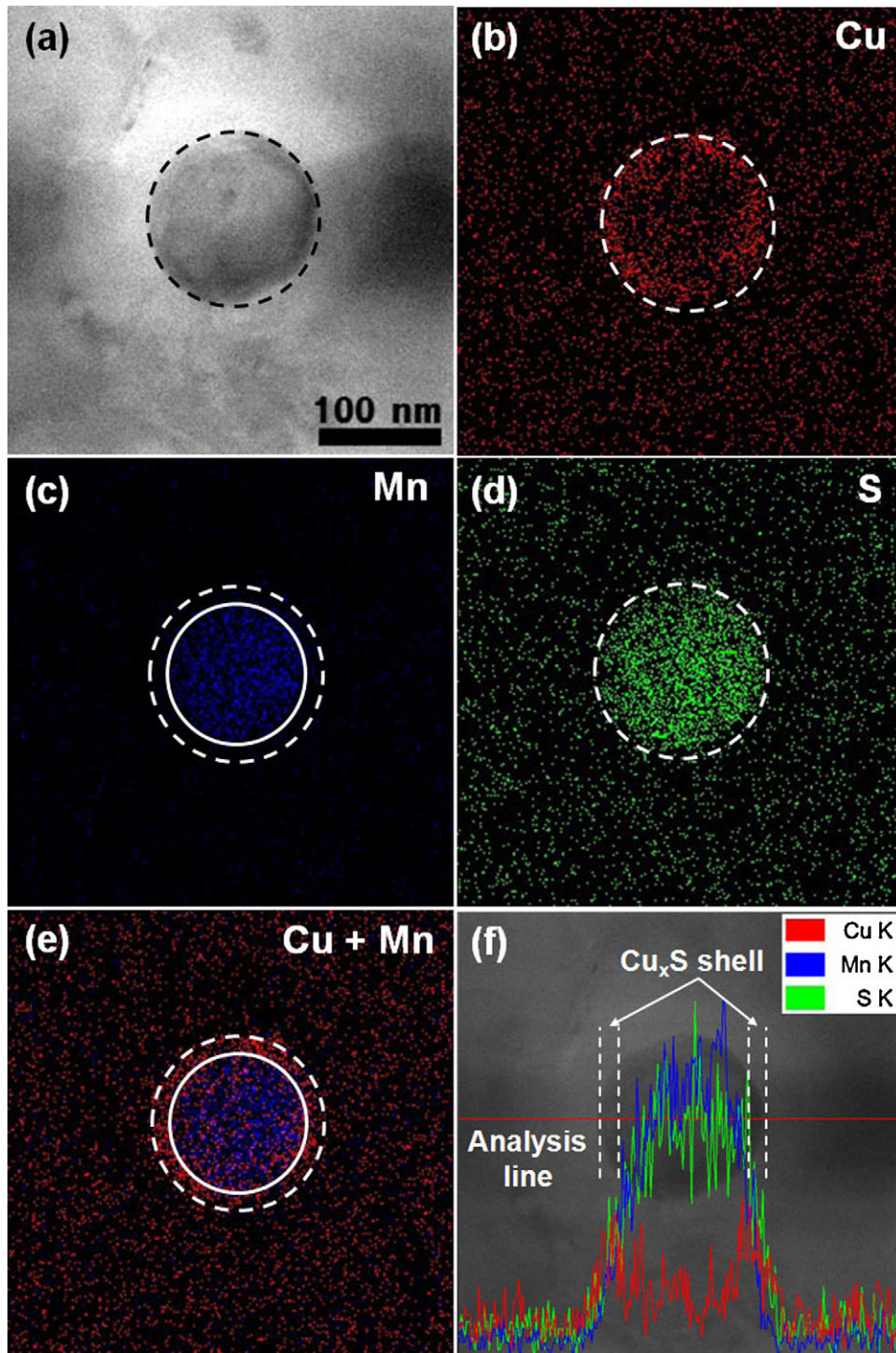| Interface	Interfacial energy, N m^{-1}
liq.Fe/liq.MnS	0.2
liq.Fe/sol.MnS	0.6
δ-Fe/sol.MnS	1.0
δ-Fe/liq.FeS	0.4
γ-Fe/sol.MnS (0 0 1)	0.712
α-Fe/sol.MnS (0 0 1)	1.024
γ-Fe/liq.Cu$_2$S	0.47
liq.Cu/liq.Cu$_2$S	0.1
γ-Fe/sol.Cu$_2$S	0.83
α-Fe/sol.Cu$_2$S	0.2

Fig. 4. (a) Scanning–TEM bright-field image, TEM/EDS elemental mapping images of (b) Cu, (c) Mn, (d) S, (e) Cu + Mn, and (f) line scanning profiles of (Cu, Mn)S in steel B.

heterogeneous precipitation of MnS can occur either at high temperature with slower cooling or where a sufficient concentration of Cu is lacking [3]. Furthermore, MnS in α-Fe has the highest growth rate, whereas Cu_2S grows more slowly than MnS in both γ-Fe and α-Fe, owing to the facts that its diffusion coefficient is the lowest in γ-Fe and its interfacial energy is the lowest in α-Fe [11]. In the present experimentation, (Cu, Mn)S precipitates were formed at high temperature, and during annealing and furnace cooling, Cu and S were slowly diffused around the existing (Cu, Mn)S at low temperature. After the cooling process, the presence of

(Cu, Mn)S precipitates of core–shell morphology in the matrix could be confirmed.

4. Conclusions

Structural characterization of precipitates in Cu bearing extra-low-carbon steels was performed by TEM/EDS and HREM. Steel C had the highest surface density, $2.19 \times 10^9 \, cm^{-2}$, and its precipitates were distributed more uniformly and densely than those of steels A or B. The (Cu, Mn)S precipitates manifested a core–shell

structure, the shell part containing Cu and S elements, and the core part Mn and S elements. The TEM analysis also revealed two nitride precipitation modes: AlN precipitates of relatively large size (several tens of nm) and elongated/cuboidal morphology, and TiN precipitates of square and rectangular shapes.

Acknowledgements

References

[1] A. Deschamps, M. Militzer, W.J. Poole, ISIJ Int. 41 (2001) 196–205.
[2] Y.R. Cho, S.I. Kim, B.S. Seong, Iron Steel Technol. 1 (2004) 46–51.
[3] Z. Liu, Y. Kobayashi, K. Nagai, ISIJ Int. 44 (2004) 1560–1567.
[4] A. Guillet, E. Es-sadipi, G. Lesperance, F.G. Hamel, ISIJ Int. 36 (1996) 1190–1198.
[5] A. Takahashi, M. Iino, ISIJ Int. 36 (1996) 241–245.
[6] P. Heritier, A. Fourdeux, Kobylanski, Scripta Metall. 15 (1981) 753–755.
[7] S. Mohamed, E. Esnouf, Acta Mater. 51 (2003) 943–957.
[8] T. Gladman, F.B. Pickering, J. Iron Steel Inst. 205 (1967) 653–664.
[9] V. Massardier, L. Voron, C. Esnouf, J. Merlin, J. Mater. Sci. 36 (2001) 1363–1371.
[10] H.H. Hong, N.H. Cho, S.I. Kim, O. Kwon, S.H. Lim, W.J. Moon, Met. Mater. Int. 16 (2010) 883–890.
[11] Z. Liu, Y. Kobayashi, K. Nagai, J. Yang, M. Kuwabara, ISIJ Int. 46 (2006) 744–753.